Informing landfill emission reporting programs through remote sensing

Katherine Howell[1], Tia R. Scarpelli[1], Riley M Duren[1], Andrew K Thorpe[2], Gregory P Asner[3], Joseph Heckler[3], Roger Green[4], Halley Brantley[4], and Daniel H. Cusworth[1]

[1]Carbon Mapper, Inc, Pasadena, CA, USA

[2]Jet Propulsion Laboratory, California Institute of Technology, Pasadena, CA, USA

[3]Arizona State University, Center for Global Discovery and Conservation Science, Tempe, AZ USA

[4]WM, Houston, TX, USA

This manuscript is a non-peer reviewed preprint submitted to EarthArXiv. The manuscript is currently under peer review at an academic journal.

Abstract

Landfills are a significant source of global methane emissions. To quantify and track emissions from these sources over time, jurisdictions and industry experts generally use emission models that involve a variety of process and waste characterization assumptions. These models are used to assess landfill operational performance and establish emission reduction targets. Testing the assumptions of these models through atmospheric measurements is challenging due to the complex nature and variability of landfill emissions, and due to difficulty in observing a sufficient set of waste sites than span a diversity of operations, sizes, and management practices. In this study, using data from multi-season campaigns with airborne and satellite remote sensing instruments in both California and the Southeastern U.S., we quantify correlation between site-level variables (operational and environmental) and observed emissions, and use this information to guide observation-informed adjustments to emissions models, reconciling the two emission estimates. Through intensive airborne sampling at California sites, we quantify variability of site-level emissions throughout the study period, yet do not find a clear seasonal pattern to this variability. We show significant correlation between measured annual gas collection as reported to the United States Greenhouse Gas Reporting Program (GHGRP) and time-averaged emissions estimates derived from airborne remote-sensing data. Observed emissions are also strongly correlated with one of the GHGRP's existing emission models but suggest that there may be a low, regionally variable, bias in the model compared to observations. We use gas collection efficiency, a key assumption to this model, as an adjustment factor to bring modeled emissions more in line with observations and test this methodology for reconciliation against varying monitoring schemes using satellite and airborne data. We find that observed and modeled emissions agree when reported collection efficiencies at individual landfills are replaced with optimized regional values (42% in the Southeast, 69% in California). These results demonstrate a pathway for top-down and bottom-up landfill emission reconciliation, helping to improve reporting and verification programs which are crucial for attributing progress towards sustainability goals.

1 Introduction

As a major contributor of anthropogenic emissions, reduction of methane emissions from the solid waste sector, including landfills, is a near-term climate strategy to reduce anthropogenic-induced warming (Ocko et al., 2021). Emissions from managed landfills manifest through a variety of pathways, including both diffuse (i.e., "area") and spatially concentrated (i.e., "point") sources. For example, emissions distributed across a landfill cover can manifest as diffuse emissions whereas point source emissions can originate from gas wells, gas destruction systems, or the active disposal area. Landfill emission models rely heavily on parameterizations, like waste decomposition timescales (IPCC, 2006, US EPA, n, d), that are difficult to validate, especially given the variety of methane sources at a landfill. Studies have shown discrepancies between modeled estimates and emission estimates derived from atmospheric observations. These studies draw on different methods and use data from a variety of approaches, including inverse modeling of total column satellite observations (e.g, Nesser et al., 2024; Wang et al., 2025), airborne and satellite point source observations (e.g. Cusworth et al., 2024; Scarpelli et al., 2024, Dogniaux et al., 2024; Zhang et al., 2025; Krause et al., 2025), and airborne in situ measurements (e.g. Catena et al., 2025), but few studies provide evidence of reconciliation of the modeled and observed estimates.

From a bottom-up modeling perspective, quantifying landfill emission behavior may require information about the deposited waste at the landfill, activities and management practices, and environmental factors. The U.S. Greenhouse Gas Reporting Program (GHGRP) requires landfills with gas collection systems to estimate their annual emissions using two different models (40 CFR Part 98). These two models differ in the way they estimate methane generation. The "recovery-first" model estimates methane generation using annual collected gas and an estimated collection efficiency while the "generation-first" model estimates methane generation based on the amount of waste present and a first order decay model. Analyses have shown cases of inconsistency between these two different reporting protocols (Balasus et al., 2025; Krause et al., 2025). While both models incorporate site-level data, including measured recovered gas and gas destruction information, neither include the workface – the active landfill area where new waste is deposited – or construction events as an explicit emission pathway. Both ground-based and airborne studies have shown large emission contributions from the workface at some landfill sites (Cusworth et al., 2020; Scarpelli et al., 2024; Risk et al., 2025),

suggesting that typical bottom-up models might be failing to account for a significant source of emissions at landfills.

From the top-down perspective, quantification of landfill emissions depends on adequate sensitivity to each emission pathway, both in spatiotemporal coverage and instrument sensitivity, along with sufficient understanding of the atmospheric conditions (e.g., wind speed) at the landfill to relate observed atmospheric concentrations to emission rates. Landfill emissions vary in time due to both operational and environmental factors and this variability must also be considered when comparing emission estimates at different timescales (i.e., models typically estimate an annual average versus observations are often a snapshot in time). Multiple studies have found a correlation between changes in atmospheric pressure and methane emissions at a mixture of closed and open landfills (Czepiel et al., 1999; Gillespie et al., 2025; Bai et al., 2025). Precipitation has been found to impact emissions from the intermediate cover – a specific component of a managed landfill system (Spokas et. al 2015). Other studies similarly note large temporal variations in landfill emissions but do not find that this variability follows a seasonal pattern (Dogniaux et al., 2024; Risk et al., 2025). Understanding temporal variability as well as adequately accounting for specific emission pathways is critical when performing model-measurement intercomparisons and when assessing potential sources of bias in either quantification approach.

Airborne imaging spectrometers have been particularly useful in expanding understanding of landfill methane emissions, as they can cover the entire site in one observation (Duren et al., 2019), while also providing sufficient spatial resolution to attribute to emissions to specific sources such as the work face or gas control infrastructure (Scarpelli et al., 2024). These instruments provide the additional benefit of spatial coverage, allowing for a broad assessment of emissions from individual landfills across states or countries (Cusworth et al., 2024; Scarpelli et al., 2024). Satellite point source imaging satellites, including Tanager-1, EMIT, EnMAP, and GHGSat, provide increased global monitoring of landfills without sacrificing the sensitivity needed to detect, quantify, and accurately attribute emissions from large waste sites (Maasakkers et al., 2022; Dogniaux et al., 2024; Zhang et al 2025; Duren et al., 2025). Quantitative emission estimates from both airborne and satellite imaging spectrometers have been compared to site-level in situ measurement approaches, suggesting that methane detected by these instruments

may in many cases be sensitive to total site emissions at large managed landfills (Cusworth et al 2024, Gillespie et al, 2025).

In this study, we use a temporally dense dataset from airborne imaging spectrometers to assess landfill emissions variability and compare to modeled annual emissions. We conducted aircraft surveys over 12 active large municipal solid waste landfills in California, repeated across multiple months in 2024. Surveys were designed to address questions of how landfill emissions variability compares to variability in operational practices and environmental conditions, as well as the representativeness of snapshot atmospheric observations in explaining annual emissions behavior. We compare observations in California, Alabama, and Georgia with key variables from bottom-up models that feed reporting programs and demonstrate a pathway to reconcile top-down and bottom-up measurements to improve assumptions about activity, collection efficiencies, and other operations that may occur systematically at landfills. We test the robustness of this reconciliation methodology against various monitoring schemes, including satellite-only monitoring using Tanager-1 and a tiered monitoring scheme combining our airborne data with satellite and in situ airborne observations.

2 Methods

2.1 Observation Strategy

Figure 1 shows intensive surveys conducted by Carbon Mapper at 12 open municipal solid waste (MSW) landfills in California in 2024 using the Global Airborne Observatory (GAO) airborne imaging spectrometer (Asner et al 2012). NASA's Airborne Visible/Infrared Imaging Spectrometer 3 (AVIRIS-3; Green et al., 2022) also flew over several of the same sites during this period. Observations from both spectrometers resulted in 4 to 18 unique survey days per site that were spread across Spring, Summer, and Fall months. Airborne observations were collected at different times of the day ranging from 10:01 – 15:47 local time. To date, the Tanager-1 satellite instrument has collected data over 14 landfills in California in 2025, with a median overpass of 12:26 local time. We additionally draw on measurements made by the satellite instrument GHGSat and airborne in-situ instrument ChampionX at three of sites. These measurements were made as part of a larger survey of landfill sites described in Krause et al 2024.

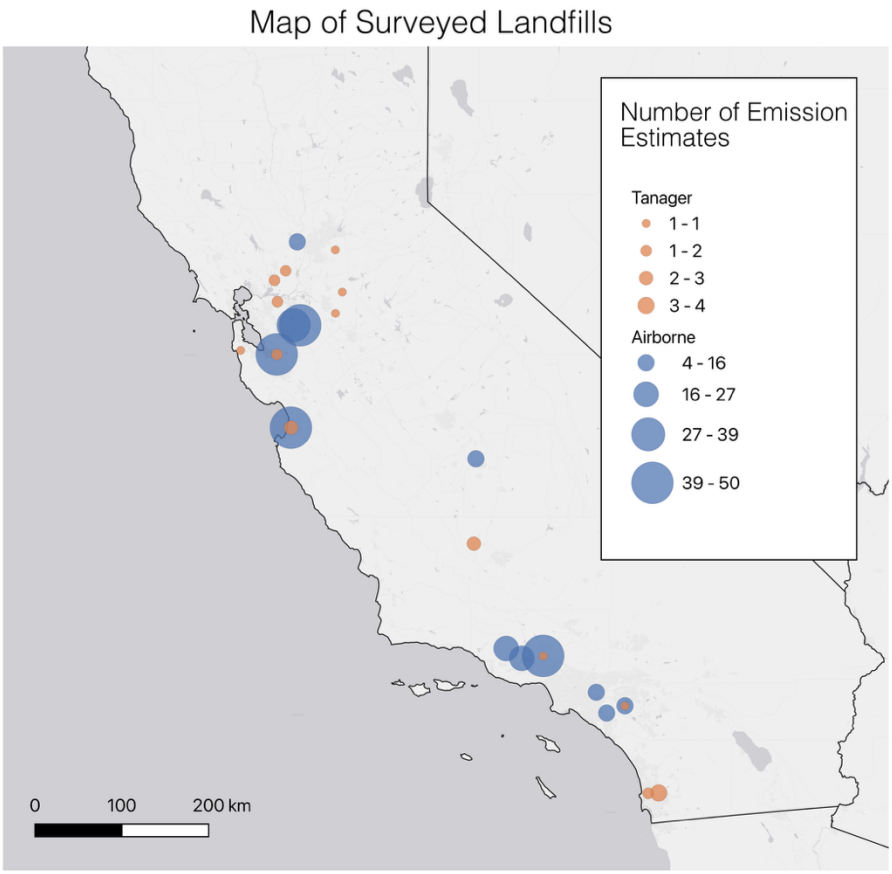

Figure 1 – Sites observed in California. Dot size corresponds to the number of quantified emission estimates at each site. Orange dots refer to Tanager-1 satellite observations for 2025, and blue dots refer to observations from 2024 multi-season airborne campaigns (GAO and AVIRIS-3).

As shown in Figure 1, sites span different regions in California. Sites surveyed in airborne campaigns were chosen to represent Californian geographic regional diversity and were observed in previous remote sensing surveys (Duren et al., 2019; Cusworth et al., 2024; Scarpelli et al., 2024). All landfills observed in California airborne campaigns have gas collection systems in place, and report waste-in-place (WIP) for 2022 between 7.8 - 92.8 x 10^6 tons, which represents 56.2 - 99.9 percentile compared to all landfills reporting to the Landfill Methane Outreach program (LMOP). Additionally, we look at annual emission estimates at a set of large active landfills in Alabama and Georgia ("Southeast") with greater than one quantified emissions estimate in 2022 (N=9). More information on this dataset and collection strategy is available in

Cusworth et al 2024. The dataset results in 1 – 5 unique survey days per site. These sites report waste-in-place (WIP) for 2022 between 5.6 – 27.1 x 10^6 tons, which represents 44.6 – 91.7 percentile compared to all landfills reporting to LMOP. Some of the California landfills are significantly larger overall compared to the Southeast (Figure S1c), yet sites observed in both regions represent a comparable sample of each region's overall population in terms of WIP (Figure S1a-b).

2.2 Methane Emission Quantification

GAO and AVIRIS-3 are passive imaging spectrometers that observe solar backscattered radiance between 400-2500 nm. AVIRIS-3 represents an advancement in optical design compared to GAO (Green et al 2022), but both instruments were fabricated in the same lab at NASA Jet Propulsion Laboratory. Tanager-1 is a newly launched satellite instrument that builds on a similar technology to the airborne imaging spectrometers (Duren et al., 2025). Column methane enhancements are retrieved from radiance using linearized matched filter approaches described in previous studies (Cusworth et al., 2024; Scarpelli et al. 2024). Detected methane plumes are segmented from background pixels using concentrations in the local neighborhood (Ayasse et al., 2024) and quantified using the concentric circle variant of the Integrated Methane Enhancement (IME) approach (Duren et al., 2019). Tanager-1 quantification methods follow a similar approach, as described in previous studies (Duren et al 2025). Methane detection and quantification methods applied to this class of airborne imaging spectrometer have been validated in blinded controlled release experiments (Ayasse et al., 2023; El Abbadi et al., 2024), and Tanager-1 methods have been validated in initial controlled release testing (Duren et al., 2025). We follow protocols to remove observations from this analysis that do not pass certain quality assessments (Carbon Mapper, 2024), which resulted in 76/382 scenes removed from analysis in this dataset.

A single landfill site often exhibits multiple distinct emitting sources that emerge from diverse activities (e.g., active waste disposal, gas collection, construction, disperse emission through the cover). In many cases, the high spatial resolution of these instruments allows for detection and quantification of distinct methane emission sources. In cases where individual emission sources are spatially distinct (i.e., their segmented plume boundaries do not overlap),

we quantify and attribute separate emission rates for each distinct plume, then sum over all source-specific plumes to estimate a site-level estimate for that overpass. However, in other cases, due to close spatial proximity of two or more individual sources, the observed plume concentration fields merge (e.g., Source 3 in Figure 2b). In this case, we detect plumes at each source and determine the total methane coming from the combination of plumes, but we cannot separately quantify and attribute the individual plume emissions at each source. To account for this behavior when calculating site level emissions, we apply the following method: if the pairwise intersection is greater than a threshold of 15%, defined as the area of the intersection over the area of the union, plumes are clustered together as illustrated in "Source 3" in Figure 2b. This threshold is chosen to distinguish between cases where segmentation successfully separates distinct sources except for lower concentration diffuse edges. As in Figure 2b, the total site level emission estimate and emission rate uncertainty is calculated by averaging individual emission rates and uncertainties in each source and then summing across sources.

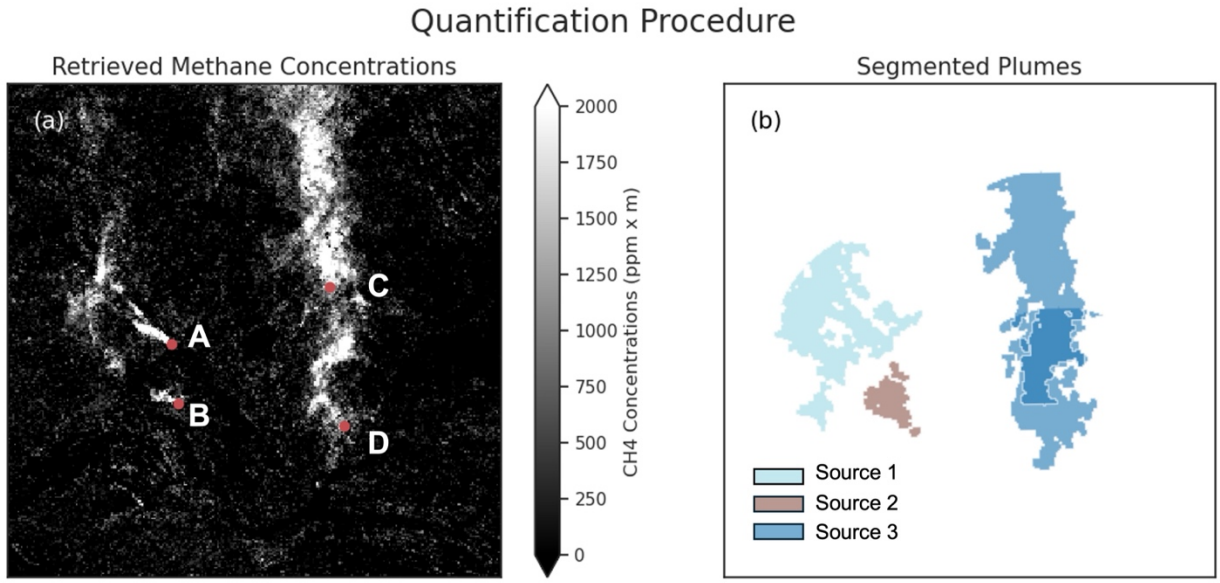

Figure 2 – Visual example of the segmentation and quantification process. (a) Retrieved methane Concentrations with identified plume origins in Red (b) Individual Plume segmentations colored by plume cluster. Given overlap individual segmentation, emission rates from points C and D are averaged, while A and B are summed. Scene level emissions estimate is the sum of Source 1, Source 2 and Source 3 emissions.

3 Results

3.1 Evaluation of Airborne Quantification Methods

We test our emission quantification approach through comparison with independent observations. Coordinated surveys were conducted in 2022 with ChampionX's (formerly Scientific Aviation) aircraft mass-balance approach at a set of landfills in Alabama and Georgia (described in more detail by Cusworth et al., 2024). Figure S2 shows the comparison between our quantification procedure and ChampionX. We find good agreement with site-level emission estimates (R^2=0.69) and overall little bias (ordinary least squares fit results in y = 0.94x - 319), highlighting the ability of this quantification approach applied to imaging spectrometer data to quantify site-level emissions for large emitting landfill sites.

3.2 Assessment of Time-Average Emission Variability

Figure 3 shows the time-series of all airborne quantified emissions observed throughout the study period. Across these 12 landfills in California, we quantified emission estimates for 306 unique complete overpasses with an average of 26 overpasses per landfill. In general, we saw persistent emissions, with total site level estimates ranging from 55 kg h^{-1} to 6654 kg h^{-1}. Figure 3 shows the coefficient of variation (COV) of emissions estimates as well as the mean relative quantified emission uncertainty at each site. The COV varies from 27%-62% across all sites, with an average value of 43%. At some sites, the COV is comparable to the average quantified uncertainty e.g. LF5, LF7, LF8, whereas other sites show more variability, with COV closer to twice the quantified uncertainty, e.g. LF6. The quantified uncertainty is a function of variability in factors that drive quantification: methane retrieval, plume segmentation processing, and wind speed. The COV is anticipated to be driven by several factors, including both quantification uncertainty and fundamental emission characteristics (barometric pressure, changes in operations, etc.). Sites where COV is significantly higher than the mean quantified uncertainties potentially represent landfills where additional factors outside quantification lead to more variability, potentially due to environmental factors (discussed in Section 3.3) or operational factors (discussed in Section 3.6). However, given rough consistency between metrics, much of the variability seen at these may be explained by quantification uncertainties.

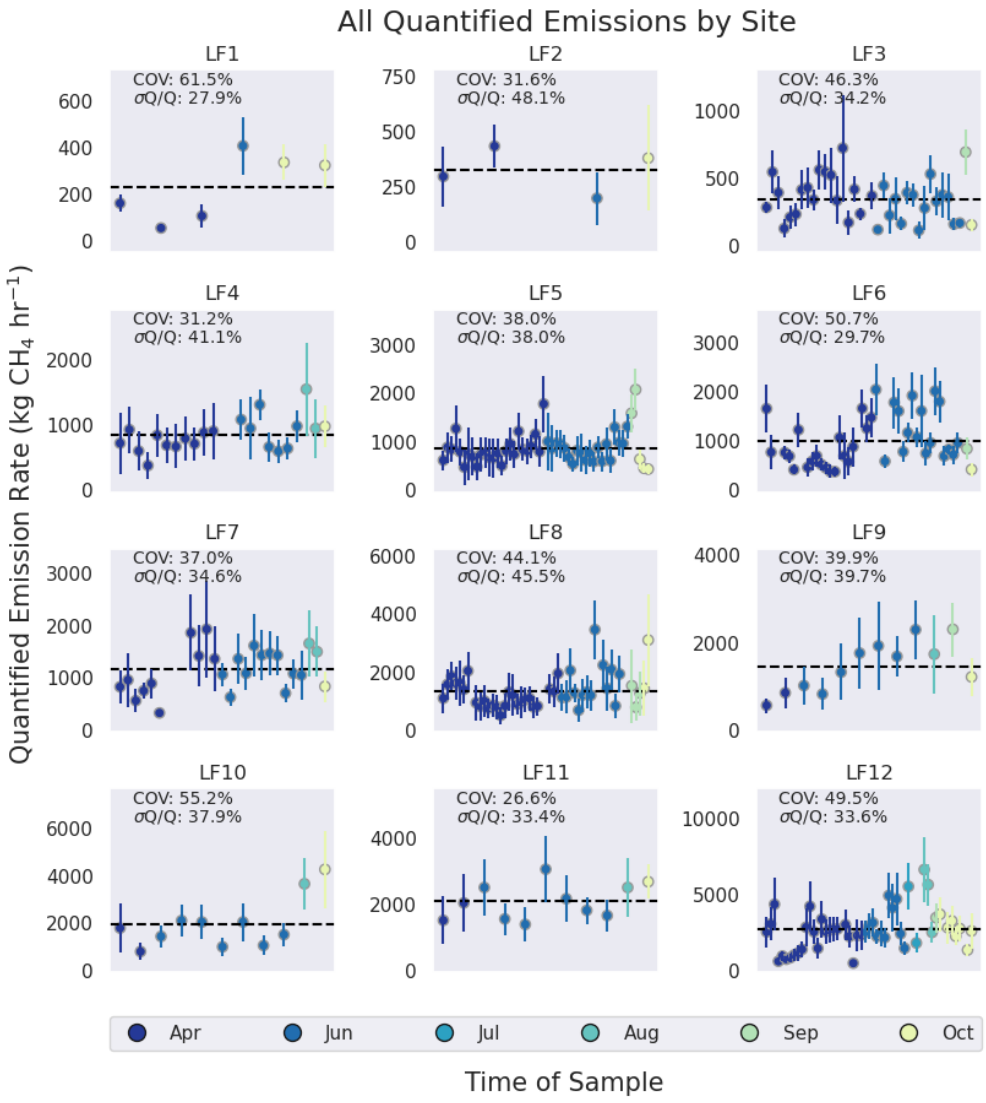

Figure 3 – All quantified emission rates at 12 surveyed sites with quantified uncertainties. Dashed lines show the mean quantified emission rate across the study period. The x-axis is not evenly spaced in time, but dots are colored by the month of observation. A version of this figure with time-justified x-axis is included in Figure S1.

GHGSat and ChampionX observed at three of these sites during the time period of our airborne survey. Figure S4 shows the full time series of daily emissions estimates at these sites. Airborne estimates are averaged across each day for direct comparison. Daily average (Figure S4) and site average (Figure S5) emission estimates show good agreement across GAO, AVIRIS-3, GHGSAT, and ChampionX, although we see a high estimate from GHGSAT at LF10 due to high daily emissions in fall tied to operational events (discussed in Section 3.6)

Consistency across sensors builds confidence that airborne estimates represent characteristic emissions and suggests that these instruments could be used in conjunction to quantify unbiased time-averaged emission estimates.

3.3 Environmental Drivers of Variability

While we see significant temporal variation in emissions at some sites in Figure 3, we do not find a statistically significant seasonal pattern in emissions across all surveyed sites. Figure 4 shows site normalized daily emissions derived from GAO/AVIRIS-3 at all sites throughout the study period, with a periodic function fit to the day of the year (Y=Acos(Bx) + C). We find low correlation, R^2=0.24, with the peak occurring around late August, due to a few spikes in emissions during this time. These spikes are likely driven by operations (discussed in more detail in section 3.6). As we do not have wintertime sampling in this study, we are not able to assess if wintertime emissions are systematically higher as previous studies have suggested (Gillespie at al., 2025; Bai et al., 2025; Catena et al 2025).

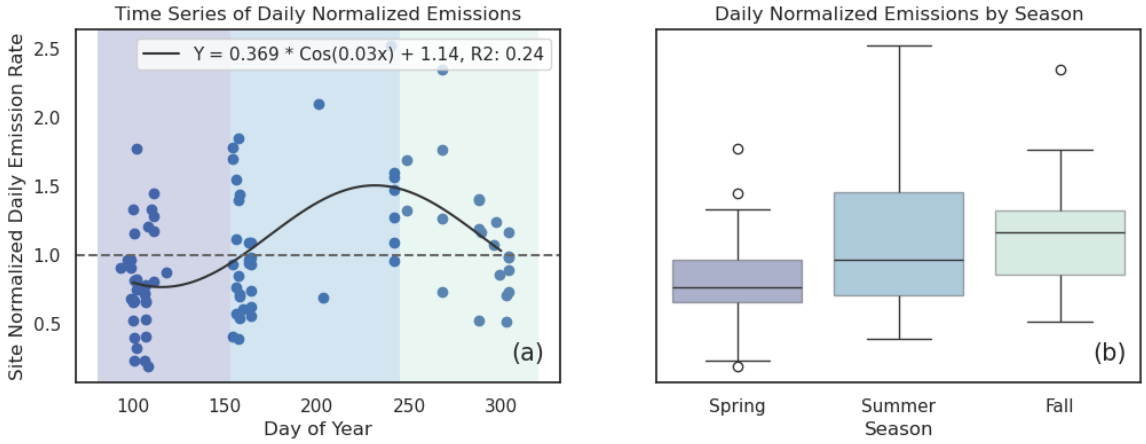

Figure 4 – Test of seasonal variability in GAO/AVIRIS-3 derived site-level emission estimates. (a) Cosine fit to site normalized emissions vs. day of the year. (b) Box plot of daily normalized emissions by season. Colors indicate season definition.

We also do not find a statistically significant correlation between site normalized daily emissions across all sites and fitted atmospheric pressure trends (Figure 5). Other studies have found a negative correlation between landfill methane emissions and changes in atmospheric pressure (Aghdam et al., 2018; Gillespie et al., 2025). Prior pressure trend is defined as the slope of a line fit to atmospheric pressure leading up to the time methane observations are made.

Atmospheric pressure is queried from the closest airport at each site (Synoptic Data, n.d., Iowa Environmental Mesonet, n.d.). This no-correlation result contrasts with previous study, indicating that drivers of variability may manifest differently across sites due to factors like climate, site design, and management practices.

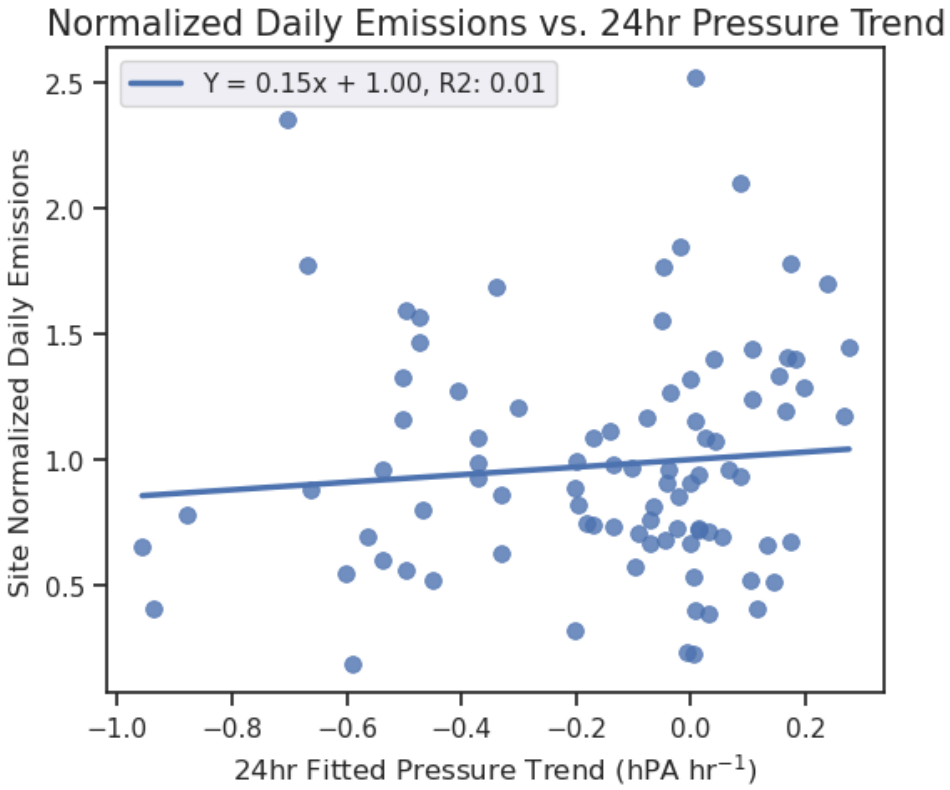

Figure 5 – Site normalized daily emissions across all California sites compared to 24hr prior fitted pressure tendency

3.3 Comparison to EPA GHGRP

We compare remote sensing-based emission estimates derived in Section 3.2 to bottom-up estimates derived via generation and recovery first protocols outlined in EPA GHGRP Subpart HH (40 CFR Part 98). Both reporting protocols for landfills with gas collection systems assume that landfill emissions follow the relationship described by Equation 1:

$$E = (G - R)(1 - OX) + D \quad (1)$$

$$G_G = f(\text{WIP}) \quad (2)$$

$$G_R = \frac{1}{C_E} R \quad (3)$$

Where E is modeled landfill emissions, R is the recovered gas measured onsite, G is modeled methane generation, D represents emissions from installed destruction devices, and OX represents the percentage of gas oxidized in the landfill cover. In practice, D and R are determined through operator reports (e.g., operator reported gas collection often based on metered flows, destruction device efficiency, and hours of downtime), and OX is assumed according to cover type (40 CFR Part 98). Modeled methane generation for generation-first models (G_G; equation 2) is estimated by inputting waste-in-place (WIP) to a first order decay model, while modeled methane generation for recovery-first models (G_R; equation 3) is estimated by dividing R by an assumed collection efficiency (C_E; ranging between 60% - 83% at airborne-surveyed sites). Different values for C_E are assumed for individual cover types, and C_E in equation 3 is calculated as an area weighted average of each of these values (table HH-3 40 CFR Part 98).

Figure 6 compares our time-averaged observed emissions at the California landfills to modeled methane generation (G_G and G_R), measured recovered gas (R), and emission estimates under both the recovery first (E_R) and generation-first (E_G) models. We use GHGRP data as reported in 2023, which is this most recent reporting year available. When we compare our remotely sensed emission estimates to bottom-up modeled emissions, we find that E_R (emissions modeled via Eqns. 1 and 3) overall shows good agreement with observed emissions (R^2=0.67) with a slight low bias compared to observations (Figure 6d). E_G (emissions modeled via Eqns. 1 and 2) shows insignificant correlation (R^2=0.10) but is unbiased compared to observations (Figure 6c). We show good correlation with modeled methane generation (G_G) and the best correlation with recovered gas (R), but these relationships deteriorate when equation 1 is applied (i.e., moving from G_G and R to E_G and E_R respectively). As our observations show better correlation with underlying variables (G_G and R) compared to modeled emission rates (E_G and E_R), there are potentially other sources of error in this emissions model as applied in equation 1. The significant correlation observed through comparison to G_G and R shows that time-averaged atmospheric observations are sensitive to distinguish site-to-site variability related to underlying operating conditions and site characteristics.

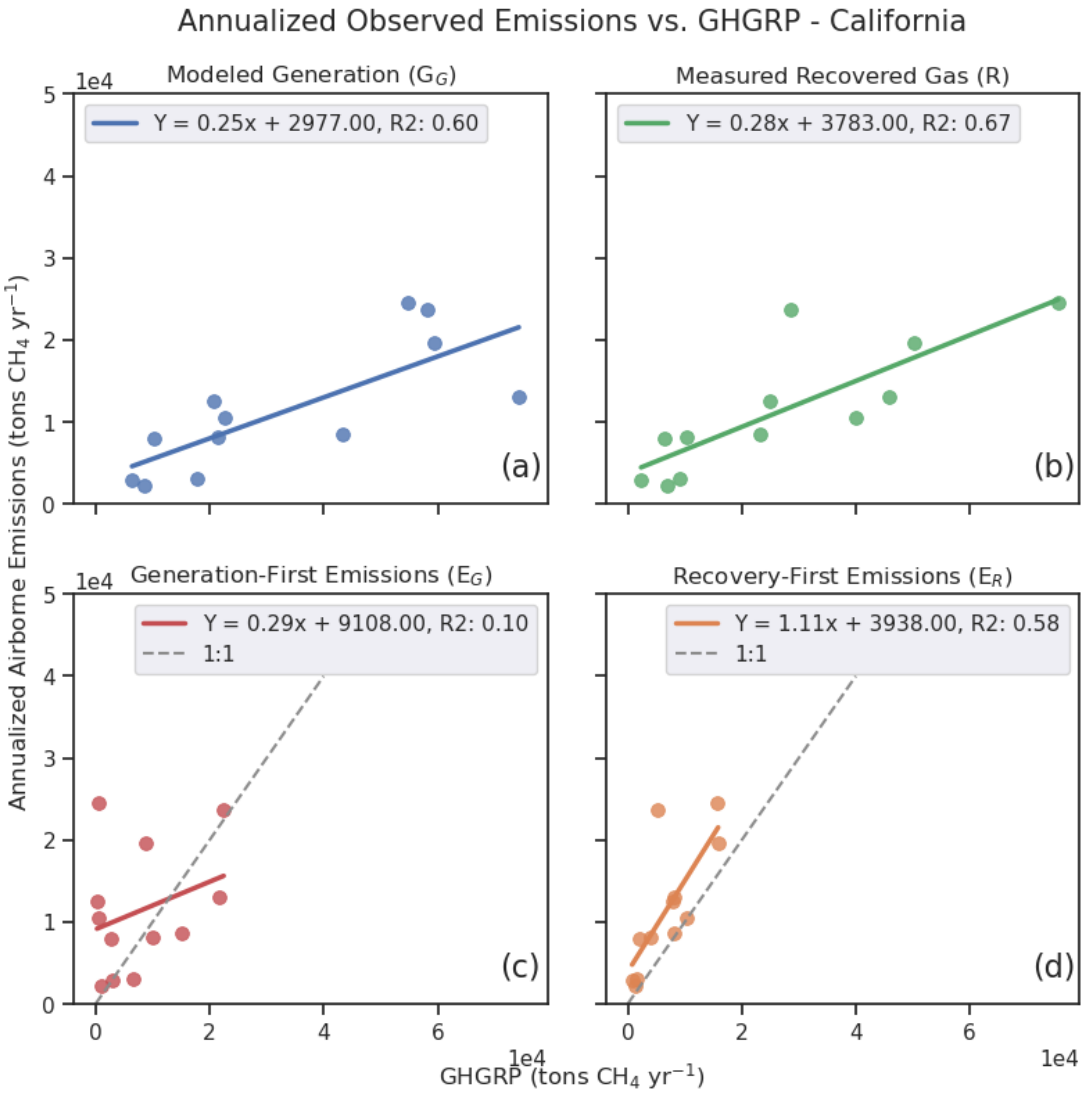

Figure 6 – Observed emissions at California sites vs values reported to the GHGRP in 2023 (a) Observed annualized emissions compared to generation-first methane generation (G_G) (b) Observed annualized emissions compared to measured recovered gas (R) (c) Observed annualized emissions compared to Generation-First emissions (E_G) (d) Observed annualized emissions compared to Recovery-First emissions (E_R)

In Figure S6, we test whether the behavior identified in Figure 6 is present outside of California by performing the same comparison of observed emissions and reported values at Southeast landfills surveyed with airborne remote sensing in 2022. As in California, we see good correlation with recovered gas (R) (R^2=0.76), again demonstrating the ability of repeat remote-sensing observations to distinguish site-to-site variability. Unlike California, Southeast observed

landfill emissions show a significant high bias compared to recovery-first modeled estimates (E_R), with observations around 4.2 times higher on average than modeled estimates. Across both regions, generation-first modeled emissions (E_G) are unbiased but show poor correlation with observations, which aligns with results of previous studies (Dogniaux et al., 2024; Krause et al., 2025). We also see significant correlation with G_G, which is calculated via WIP (equation 2), consistent with results of a recent study (Krause et al., 2025).

3.4 Reconciling top-down and bottom-up emission estimates

The bias between our observed emissions and E_R could be the result of several factors, including sampling limitations (e.g., unquantified temporal variability due to daytime-only sampling) or reporting model biases (e.g., underestimated modeled emissions due to incorrect assumptions about collection efficiencies). Though we do not see evidence of pressure tendency effects on observed emission estimates based on daytime sampling (Figure 5), other studies have indicated overestimation in landfill emissions could result from instruments that only sample in the daytime (Delkash et al., 2022.) which could potentially explain some of the bias between observed and modeled E_R emissions in Figure 6d and Figure S6d.

If instead we assume that the bias is driven by inaccurate collection efficiencies (C_E), we can use our observational data to guide adjustments of C_E that bring modeled and observed estimates more in line. First, we optimize a single regionally specific collection efficiency by minimizing the bias between our observed values and E_R (using equation 1 and 3). This procedure yields a remote sensing-derived C_E of 69% at California sites and 42% at Southeast sites. We then calculate new E_R estimates ("Reconciled E_R") by replacing the site-level reported collection efficiencies with our regional optimized collection efficiencies (Figure 7c-d).

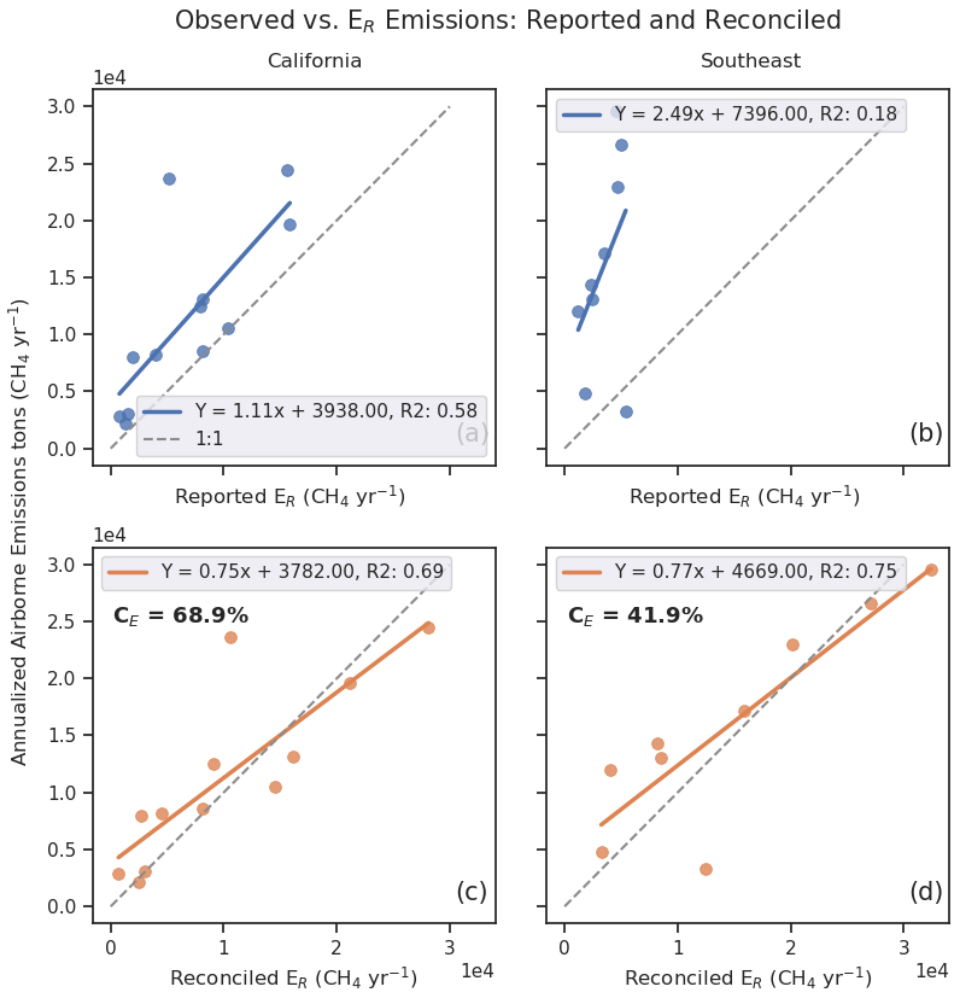

Figure 7 – (a) Observed annualized emissions in California compared to recovery-first methane emissions, same as Figure 6d (b) and Southeast, same as Figure S5d (c) Observed annualized emissions in California compared to reconciled recovery-first emissions as described in section 3.2 (d) and Southeast

Figure 8 shows the 95% confidence interval on each empirically derived C_E. While this confidence interval overlaps reported values at sites in California, this is not the case in the Southeast. To bring modeled emissions (E_R) in line with observations in the Southeast we must use a regional collection efficiency that is statistically different from reported values, which could suggest that collection efficiency is overestimated at sites in the Southeast. There are various possible explanations for why collection efficiency may vary between these two regions. For example, they have differing climate conditions, such as significantly higher rainfall in the

Southeast than in California (Figure S7), as well as differing regulatory environments (CARB, n.d.) which may impact management practices. Here we assumed the top-down versus bottom-up differences are due to bottom-up model bias (i.e., due to inaccuracy of assumed collection efficiency), but continued study with more detailed site-level information is needed to uncover whether these lingering differences are driven more by observational or model bias.

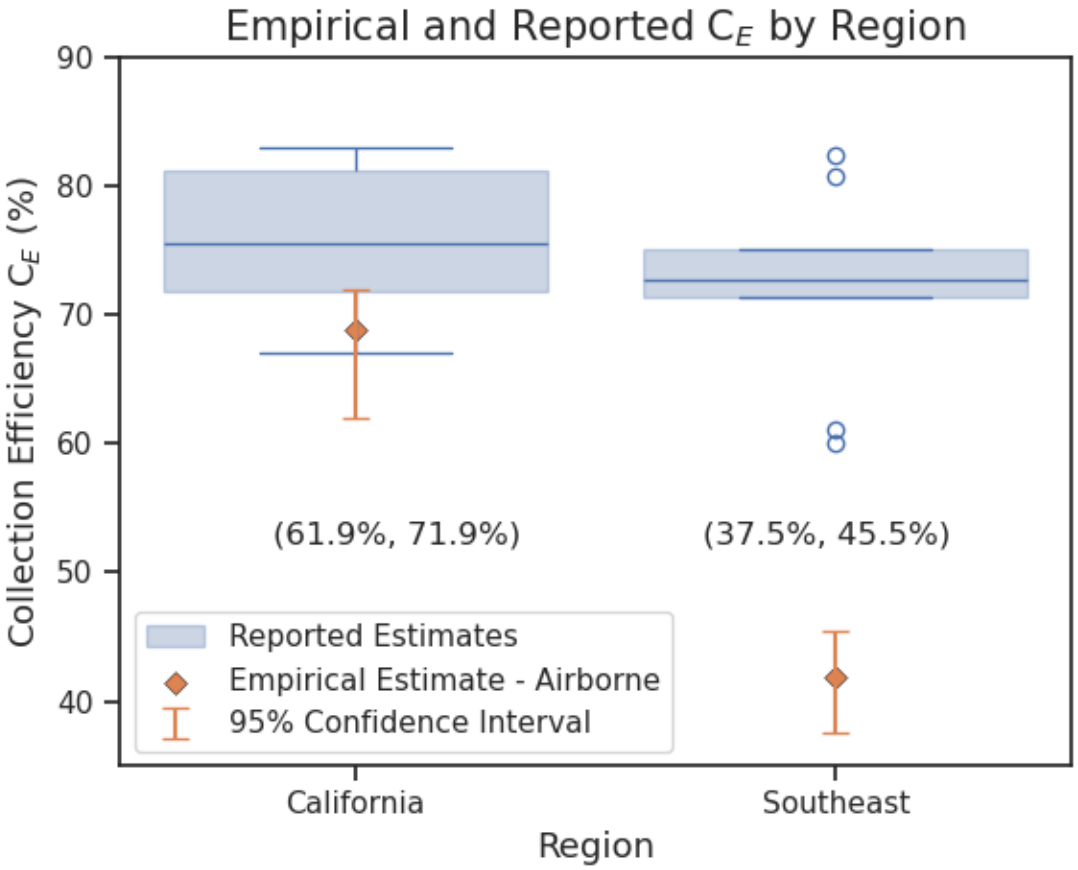

Figure 8 – Blue box plot shows reported gas collection efficiencies by region. Orange points represent the empirically estimated collection efficiency in each region, and orange lines indicate the 95% confidence interval obtained through bootstrapping.

3.5 Applicability of satellites for emission reconciliation

Point source imaging satellites also have demonstrated capability to quantify large emissions from landfill sources, albeit at a coarser spatial resolution and lower detection sensitivity than similar technology deployed on aircraft (Dogniaux et al., 2024; Zhang et al 2025; Krause et al., 2025). Here we assess Tanager-1 observations at landfills in California (Figure 1). Given the recent launch and commissioning activities extending through early 2025, Tanager-1

has collected limited data over California landfills. We use this initial data to assess if satellite observations with limited temporal sampling reproduce the same results as our airborne observations. Despite the more limited temporal sampling, the landfills observed with Tanager-1 are more spatially comprehensive and represent a different population of sites across California, with only 4 of the 14 Tanager-observed landfills included in our airborne surveys (Figure 1). When compared to GHGRP modeled emission estimates, quantified Tanager-1 emissions present similar correlation to airborne observations (Figure S8). Following the same reconciliation procedure as Figure 7, but using only Tanager-1 emission estimates, we find an empirical regional collection efficiency of 67% (Figure 9), which is consistent with the 69% derived from the full 2024 airborne dataset (Figure 7c). This result suggests that reduced temporal sampling may be acceptable to reconcile top-down and bottom-up emissions presuming a large observed spatial sampling of sites.

We test the impact of reduced temporal sampling by downsampling the airborne dataset in California. Figure S9 demonstrates this downsampling of the GAO/AVIRIS-3 observations at a sampling rate of once per quarter and once per year per site. Figure S9 shows that when we downsample to a single observation per quarter we still find good correlation with recovered gas (R^2=0.61) and our reconciled C_E of 71.1% is consistent with our full airborne dataset (68.9%), indicating that once per quarter sampling may be sufficient for this methodology, presuming multiple sites are surveyed within that quarter.

We further estimate C_E through a combination of all observation datasets available in this study: GAO, AVIRIS-3, Tanager-1, GHGSAT, and ChampionX (combining data from Figure 1 and Figure S3). We follow the same procedure to estimate C_E, instead averaging emission estimates across all instruments. Although GHGSAT and ChampionX datasets have significant temporal sampling, we do not calculate instrument specific regional collection efficiencies for them given limited spatial sampling. By including data from all instruments described in this study, we find a consistent regional C_E (69%; Figure 9) and good correlation with recovered gas (R^2=0.64; Figure S10), despite an increased diversity of sites (N=22). When using all instruments, we find the tightest confidence interval (65.0%, 72.5%), likely reflecting the high spatial and temporal sampling of this combined dataset. Regardless of varied spatial sampling, temporal sampling, and instrument detection sensitivities, the regional California C_E estimate is consistent, indicating the robustness of this reconciliation method.

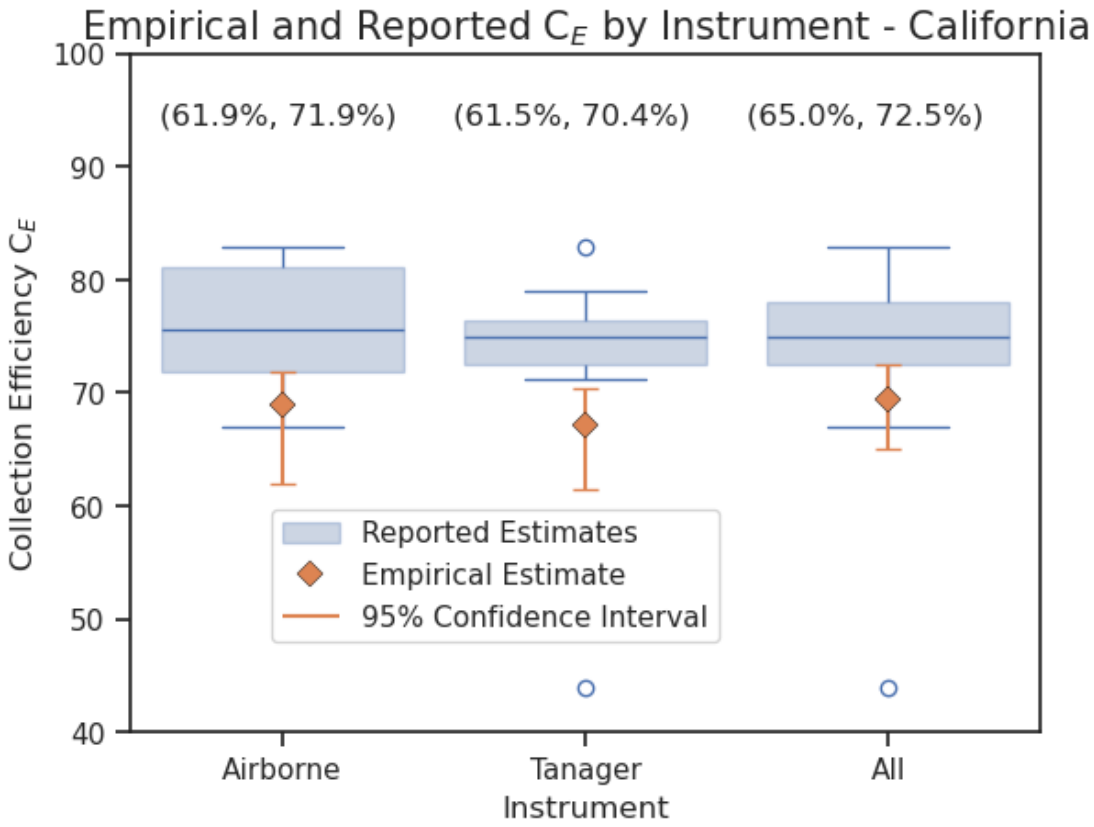

Figure 9 – Comparison of reported and derived collection efficiencies. Box plots showing reported gas collection efficiencies by instrument. Orange points represent the empirically estimated collection efficiency using each instrument, and orange lines indicate the 95% confidence interval obtained through bootstrapping. The rightmost boxplot includes data from all instruments (Airborne, Tanager-1, GHGSAT and ChampionX)

3.6 Identification of operational drivers of variability

Though we do not find strong evidence for environmental drivers of variability at the landfills observed in this study, we do see examples of operations impacting short-term emission variability. In Figure S11, airborne observations at LF12 provide an example where operational influences may explain large spikes in quantified emissions. There is visual evidence of pressurized point source emissions that clearly appear on August 27th, 2024, but then disappear on August 30th. This behavior directly manifests in a spike in quantified emission rates seen in Figure S11.

Figure S12 shows a similar example of anomalous conditions at LF10. There was a spike in emissions at LF10 quantified by AVIRIS-3, GHGSat, and ChampionX during the latter half of

October, 2024, corresponding to these anomalous conditions, as shown in Figure 10. In this case, monthly gas collection supplied by the operator shows that these elevated emissions correspond to a decrease in gas collection in October and November of 2024 (Figure 10a), which was a result of short-lived maintenance after excess liquids from heavy rain impaired the gas collection system. Across 11 months of observations between the three instruments, we see significant negative correlation (R^2=0.66) between monthly quantified methane emissions and same-month operator reported gas collection (Figure 10b), suggesting that operational factors explain this temporal variability in emissions.

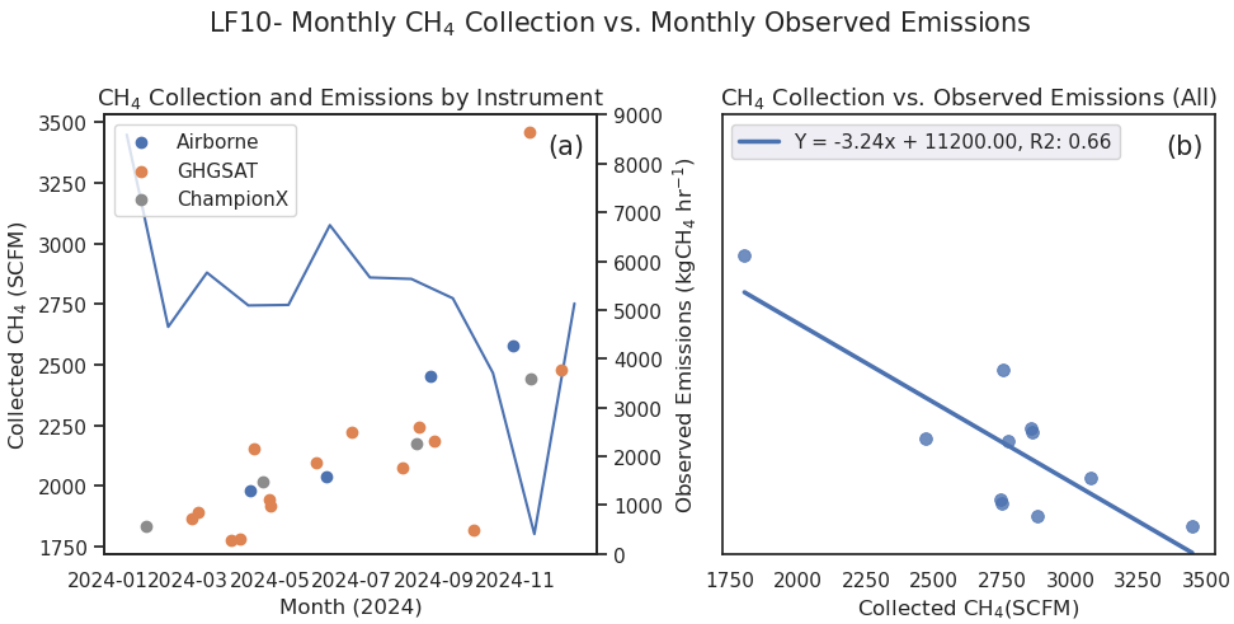

Figure 10 – Monthly gas collection and emissions by instrument for LF10. (a) Blue line shows operator recorded collected methane across all months in 2024. Dots correspond to monthly average quantified emission rates and are colored by instrument. (b) Observed monthly emissions across all instruments compared to operator recorded collected methane.

Factors such as operationally driven emission events (Figure S10, Figure S11) or quantification issues (e.g., from wind products or topography) can contribute to variability in snapshot emission estimates at individual sites (average emissions COV around 43% across all sites in Figure 3), and without operator provided information to contextualize anomalous events (as in Figure 10), single snapshot estimates might lead to overestimated annual emissions at individual landfills. However, we generally find consistent results across sampling schemes for the empirically derived regional C_E in California: the full observational dataset (69%), the full

airborne dataset (69%), one airborne sample per quarter (71%), and Tanager-1 (67%). This suggests that by observing a critical set of landfills, each at a minimum temporal cadence, snapshot observations can yield a representative assessment of annual average landfill behavior for a given region.

4 Discussion

Airborne observations between the spring and fall of 2024 show generally large emission variability at nearly all surveyed landfills, yet do not indicate that environmental factors drive emissions at large landfills in California. We find the best agreement between observations and reported metrics of annual average site operations, i.e. modeled methane generation and recovered gas collection. Many studies have highlighted discrepancies between empirical and reported estimates of landfill emissions, yet few have shown significant correlation between the two (Krause et al., 2025). This work suggests that site-level time-averaged emissions derived from airborne remote sensing are highly correlated with the GHGRP's recovery-first model. Observationally informed collection efficiencies from remote sensing observations show promise for reconciling emissions models.

Results suggest that provided sufficient spatial sampling, once per quarter (i.e., three-month) sampling is sufficient to estimate average regional collection efficiency for large landfills in California. We demonstrate robust results across instruments with different detection sensitivities: airborne imaging spectrometers, satellite imaging spectrometers, and airborne in situ instruments. However, characterization of detection limits for landfills is critical to incorporating remotely sensing data into bottom-up models. Future work is needed to estimate detection limits specific to landfill environments that can capture complexity of observing conditions (i.e. wind speed, surface brightness, topography).

Our empirically derived collection efficiencies (69% in California and 42% in the Southeast) differ from average regional reported values (76% in California and 72% in the Southeast), suggesting that collection is more efficient in California and that assumed collection efficiencies may be leading to underestimated emissions in the Southeast. This is consistent with other studies that applied inverse analysis of TROPOMI data to estimate landfill emissions in the Southeast and in select urban regions (Balasus et al., 2024; Wang et al., 2025). Deriving

collection efficiencies from daytime remote sensing observations carries uncertainty due to potential diurnal variability in landfill emissions (e.g., Delkash et al., 2022), or due to the potential effect of wintertime sampling (e.g. Gillespie et al., 2025). Continued assessment of how these factors influence variability at large landfills with gas collection systems is necessary to properly base empirically derived collection efficiencies from atmospheric observations.

More work is needed to understand to what degree regional operational and management practices (e.g., prevalence of construction events, work face emissions), regulatory environments, and regional climate characteristics contribute to this finding. In this study we primarily focus on California, a region with a milder climate compared to regions investigated in other studies (Gillespie et al 2025, Bai et al., 2025). Satellites that can provide high spatial sampling across different regions are well suited to further characterize variability in landfill emissions. Datasets spanning multiple regions with varied climates, management, and regulatory environments will help uncover how these factors influence emissions. Such datasets could help ensure that bottom-up model parameterizations are capturing key drivers of site-to-site emissions variability (i.e. annual rainfall, characteristics of the landfill workface, etc.) and could inform a global framework for reconciling top-down and bottom-up emissions estimates.

References

40 CFR Part 98 2009 Mandatory Greenhouse Gas Reporting (United States Code of Federal Regulations; www.ecfr.gov/current/title-40/part-98, last access: July 29, 2025.

Aghdam, E.F., Fredenslund, A.M., Chanton, J., Kjeldsen, P., Scheutz, C., 2018. Determination of gas recovery efficiency at two Danish landfills by performing downwind methane measurements and stable carbon isotopic analysis. Waste Management 73, 220–229. https://doi.org/10.1016/j.wasman.2017.11.049

Asner, G.P., 2007. Carnegie Airborne Observatory: in-flight fusion of hyperspectral imaging and waveform light detection and ranging for three-dimensional studies of ecosystems. J. Appl. Remote Sens 1, 013536. https://doi.org/10.1117/1.2794018

Ayasse, A.K., Cusworth, D., O'Neill, K., Fisk, J., Thorpe, A.K., Duren, R., 2023. Performance and sensitivity of column-wise and pixel-wise methane retrievals for imaging spectrometers. Atmos. Meas. Tech. 16, 6065–6074. https://doi.org/10.5194/amt-16-6065-2023

Bai, S., Li, F., Yan, Y., Huang, Q., Jiang, F., Chen, H., Zhang, Y., 2025. Seasonal Variations of Methane Emissions from a Urumqi Landfill in China and its driving factors using Hyperspectral Satellite Time-Series Observations. https://doi.org/10.22541/essoar.174180717.78491070/v1

Balasus, N., Jacob, D.J., Maxemin, G., Jenks, C., Nesser, H., Maasakkers, J.D., Cusworth, D.H., Scarpelli, T.R., Varon, D.J., Wang, X., 2025. Satellite monitoring of annual US landfill methane emissions and trends. Environ. Res. Lett. 20, 024007. https://doi.org/10.1088/1748-9326/ada2b1

California Air Resources Board (CARB), n.d. Landfill Methane Regulation. Available at: https://ww2.arb.ca.gov/our-work/programs/landfill-methane-regulation [Accessed 29 July. 2025].

Carbon Mapper, 2024. Carbon Maper Quality Control Description Document. Available at: https://assets.carbonmapper.org/documents/Carbon-Mapper-Plume-Detection-Quality-Control-Public.pdf [Accessed 29 July. 2025]

Catena, A.M., Smith, M.L., Murray, L.T., Leibensperger, E.M., Zhang, J., Schwab, M.J., Schwab, J.J., 2025. Aerial Estimates of Methane and Carbon Dioxide Emission Rates Using a Mass Balance Approach in New York State. https://doi.org/10.5194/essd-2025-135

Cusworth, D.H., Duren, R.M., Ayasse, A.K., Jiorle, R., Howell, K., Aubrey, A., Green, R.O., Eastwood, M.L., Chapman, J.W., Thorpe, A.K., Heckler, J., Asner, G.P., Smith, M.L., Thoma, E., Krause, M.J., Heins, D., Thorneloe, S., 2024. Quantifying methane emissions from United States landfills. Science 383, 1499–1504. https://doi.org/10.1126/science.adi7735

Cusworth, D.H., Duren, R.M., Thorpe, A.K., Tseng, E., Thompson, D., Guha, A., Newman, S., Foster, K.T., Miller, C.E., 2020. Using remote sensing to detect, validate, and quantify methane emissions from California solid waste operations. Environ. Res. Lett. 15, 054012. https://doi.org/10.1088/1748-9326/ab7b99

Czepiel, P.M., Shorter, J.H., Mosher, B., Allwine, E., McManus, J.B., Harriss, R.C., Kolb, C.E., Lamb, B.K., 2003. The influence of atmospheric pressure on landfill methane emissions. Waste Management 23, 593–598. https://doi.org/10.1016/S0956-053X(03)00103-X

Delkash, M., Chow, F.K., Imhoff, P.T., 2022. Diurnal landfill methane flux patterns across different seasons at a landfill in Southeastern US. Waste Management 144, 76–86. https://doi.org/10.1016/j.wasman.2022.03.004

Dogniaux, M., Maasakkers, J., Girard, M., Jervis, D., McKeever, J., Schuit, B., Sharma, S., Lopez-Noreña, A., Varon, D., Aben, I., 2024. Satellite survey sheds new light on global solid waste methane emissions. https://doi.org/10.31223/X5TB09

Duren, R., Cusworth, D., Ayasse, A., Howell, K., Diamond, A., Scarpelli, T., Kim, J., O'neill, K., Lai-Norling, J., Thorpe, A., Zandbergen, S.R., Shaw, L., Keremedjiev, M., Guido, J., Giuliano, P., Goldstein, M., Nallapu, R., Barentsen, G., Thompson, D.R., Roth, K., Jensen, D., Eastwood, M., Reuland, F., Adams, T., Brandt, A., Kort, E.A., Mason, J., Green, R.O., 2025. The Carbon Mapper emissions monitoring system. https://doi.org/10.5194/egusphere-2025-2275

Duren, R.M., Thorpe, A.K., Foster, K.T., Rafiq, T., Hopkins, F.M., Yadav, V., Bue, B.D., Thompson, D.R., Conley, S., Colombi, N.K., Frankenberg, C., McCubbin, I.B., Eastwood, M.L., Falk, M., Herner, J.D., Croes, B.E., Green, R.O., Miller, C.E., 2019. California's methane super-emitters. Nature 575, 180–184. https://doi.org/10.1038/s41586-019-1720-3

El Abbadi, S.H., Chen, Z., Burdeau, P.M., Rutherford, J.S., Chen, Y., Zhang, Z., Sherwin, E.D., Brandt, A.R., 2024. Technological Maturity of Aircraft-Based Methane Sensing for Greenhouse Gas Mitigation. Environ. Sci. Technol. 58, 9591–9600. https://doi.org/10.1021/acs.est.4c02439

Gillespie, L.D., Ars, S., Alkadri, S., Urya, S., Khoo, T., Fraser, S., Vogel, F., Wunch, D., 2025. Estimating methane emissions from the waste sector in Southern Ontario using atmospheric measurements. Journal of the Air & Waste Management Association 75, 144–163. https://doi.org/10.1080/10962247.2024.2435340

Green, R.O., Schaepman, M.E., Mouroulis, P., Geier, S., Shaw, L., Hueini, A., Bernas, M., McKinley, I., Smith, C., Wehbe, R., Eastwood, M., Vinckier, Q., Liggett, E., Zandbergen, S., Thompson, D., Sullivan, P., Sarture, C., Van Gorp, B., Helmlinger, M., 2022. Airborne Visible/Infrared Imaging Spectrometer 3 (AVIRIS-3), in: 2022 IEEE Aerospace Conference (AERO). Presented at the 2022 IEEE Aerospace Conference (AERO), IEEE, Big Sky, MT, USA, pp. 1–10. https://doi.org/10.1109/AERO53065.2022.9843565

Hasan, Md.H., Zhang, P., Chen, J., Shi, G., Abichou, T., Yu, H., 2025. Exploring uncertainties in the integrated mass enhancement method for remote sensing retrievals of methane emissions. Waste Management 200, 114759. https://doi.org/10.1016/j.wasman.2025.114759

Iowa Environmental Mesonet (IEM), n.d. Archived weather data [Dataset]. Iowa State University. Available at: https://mesonet.agron.iastate.edu/request/download.phtml [Accessed 29 July. 2025].

IPCC, 2006. Chapter 5: Waste. In: 2006 IPCC Guidelines for National Greenhouse Gas Inventories, Volume 5: Waste. Intergovernmental Panel on Climate Change. Available at: https://www.ipcc.ch/site/assets/uploads/2018/03/5_Waste-1.pdf [Accessed 29 July. 2025].

Krause, M.J., Thoma, E.D., Bryant, A., Brantley, H., MacDonald, M., Green, R., Thorneloe, S., 2025. A High-Resolution Satellite Survey of Methane Emissions from 60 North

American Municipal Solid Waste Landfills. Environ. Sci. Technol. 59, 15080–15091. https://doi.org/10.1021/acs.est.5c01409

Maasakkers, J.D., Varon, D.J., Elfarsdóttir, A., McKeever, J., Jervis, D., Mahapatra, G., Pandey, S., Lorente, A., Borsdorff, T., Foorthuis, L.R., Schuit, B.J., Tol, P., Van Kempen, T.A., Van Hees, R., Aben, I., 2022. Using satellites to uncover large methane emissions from landfills. Sci. Adv. 8, eabn9683. https://doi.org/10.1126/sciadv.abn9683

Nesser, H., Jacob, D.J., Maasakkers, J.D., Lorente, A., Chen, Z., Lu, X., Shen, L., Qu, Z., Sulprizio, M.P., Winter, M., Ma, S., Bloom, A.A., Worden, J.R., Stavins, R.N., Randles, C.A., 2024. High-resolution US methane emissions inferred from an inversion of 2019 TROPOMI satellite data: contributions from individual states, urban areas, and landfills. Atmos. Chem. Phys. 24, 5069–5091. https://doi.org/10.5194/acp-24-5069-2024

NOAA National Centers for Environmental Information. (2021). U.S. Climate Normals:Annual Precipitation for 2006–2020 (15-year period) [Dataset]. U.S. Department of Commerce. https://www.ncei.noaa.gov/access/us-climate-normals/ [Accessed 29 July. 2025].

Ocko, I.B., Sun, T., Shindell, D., Oppenheimer, M., Hristov, A.N., Pacala, S.W., Mauzerall, D.L., Xu, Y., Hamburg, S.P., 2021. Acting rapidly to deploy readily available methane mitigation measures by sector can immediately slow global warming. Environ. Res. Lett. 16, 054042. https://doi.org/10.1088/1748-9326/abf9c8

Risk, D., Omidi, A., Bourlon, E., Khaleghi, A., Perrine, G., Tarakki, N., Martino, R., Stuart, J., 2025. Active Face Emissions: An Opportunity for Reducing Methane Emissions in Global Waste Management. https://doi.org/10.31223/X5GB1K

Scarpelli, T.R., Cusworth, D.H., Duren, R.M., Kim, J., Heckler, J., Asner, G.P., Thoma, E., Krause, M.J., Heins, D., Thorneloe, S., 2024. Investigating Major Sources of Methane Emissions at US Landfills. Environ. Sci. Technol. 58, 21545–21556. https://doi.org/10.1021/acs.est.4c07572

Spokas, K., Bogner, J., Corcoran, M., Walker, S., 2015. From California dreaming to California data: Challenging historic models for landfill CH4 emissions. Elementa: Science of the Anthropocene 3, 000051. https://doi.org/10.12952/journal.elementa.000051

Synoptic Data, n.d. MesoWest METAR weather observations [Dataset]. University of Utah. Available at: https://synopticdata.com/mesowest-users/ [Accessed 29 July. 2025].

US EPA Greenhouse Gas Reporting Program (GHGRP); https://www.epa.gov/ghgreporting, last access: July 29, 2025.

US EPA LFG Energy Project Development Handbook, Landfill Methane Outreach Program (LMOP); United States Environmental Protection Agency, 2024. https://www.epa.gov/system/files/documents/2024-01/pdh_full.pdf, last access: July 29, 2025.

U.S. EPA, n.d. Waste Reduction Model (WARM). Available at: https://www.epa.gov/waste-reduction-model [Accessed 29 July. 2025].

Wang, X., Jacob, D.J., Nesser, H., Balasus, N., Estrada, L., Sulprizio, M., Cusworth, D.H., Scarpelli, T.R., Chen, Z., East, J.D., Varon, D.J., 2025. Quantifying urban and landfill methane emissions in the United States using TROPOMI satellite data. https://doi.org/10.48550/ARXIV.2505.10835

Zhang, S., Lei, M., Huang, X., Zhang, Y., 2025. Evaluation of methane emission from MSW landfills in China, India, and the U.S. from space using a two-tier approach. Journal of Environmental Management 377, 124705. https://doi.org/10.1016/j.jenvman.2025.124705

Zhang, X., Maasakkers, J., Roger, J., Guanter, L., Sharma, S., Lama, S., Tol, P., Varon, D., Cusworth, D., Howell, K., Thorpe, A., Brodrick, P., Aben, I., 2024. Global identification of solid waste methane super emitters using hyperspectral satellites. https://doi.org/10.31223/X57132

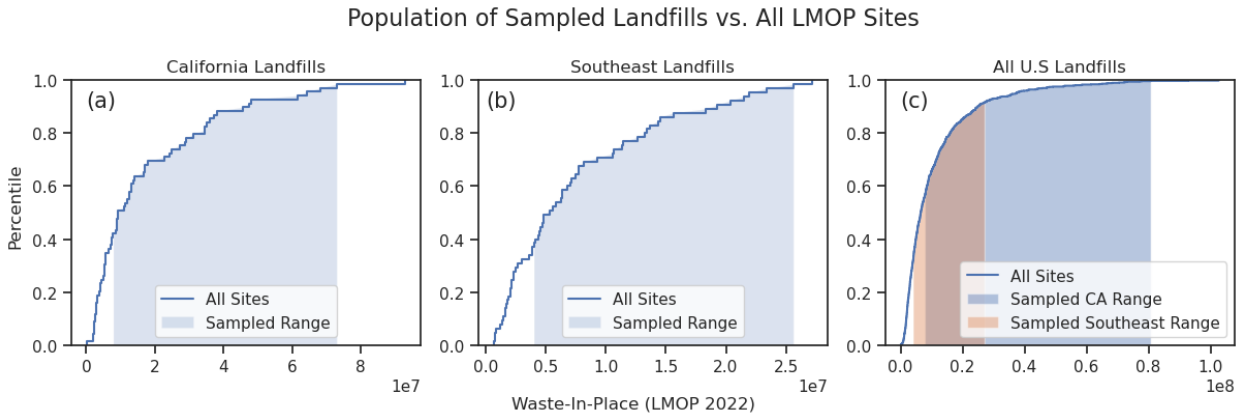

Figure S1 – (a) Blue line shows the cumulative distribution of Waste-In-Place for all Landfill Methane Outreach program (LMOP) sites in California. The shaded blue area represents the range of Waste-In-Place values for observed sites. (b) Shows the same as 3a for Southeast sites. (c) Blue Line represents the cumulative distribution of WIP for all landfills reporting to LMOP. Orange shaded region represents sites observed in the Southeast and blue shaded region represents sites observed in California.

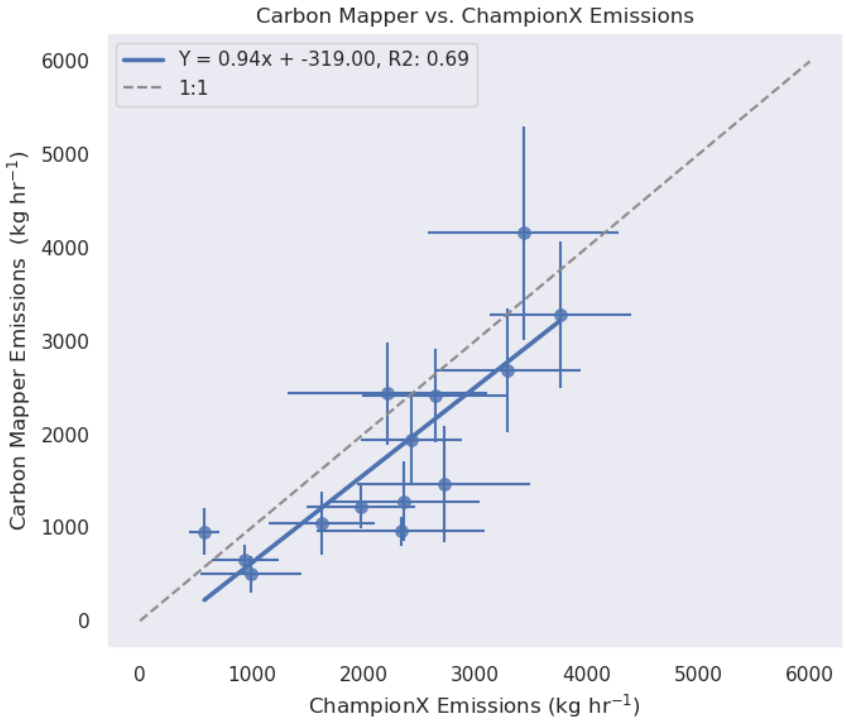

Figure S2 – Carbon Mapper emission rates using outlined methods vs. ChampionX emission rates

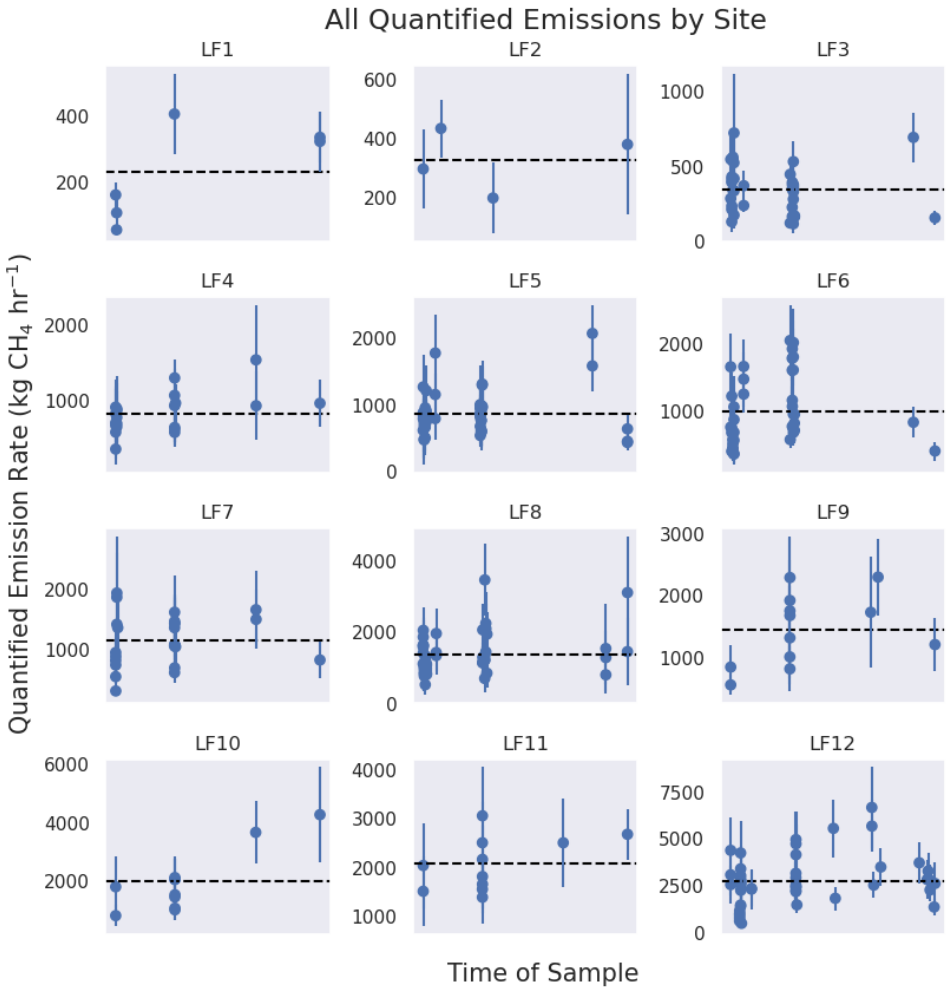

Figure S3 – All quantified emission rates at surveyed sites with quantified uncertainties. Dashed lines show the mean quantified emission rate across the study period.

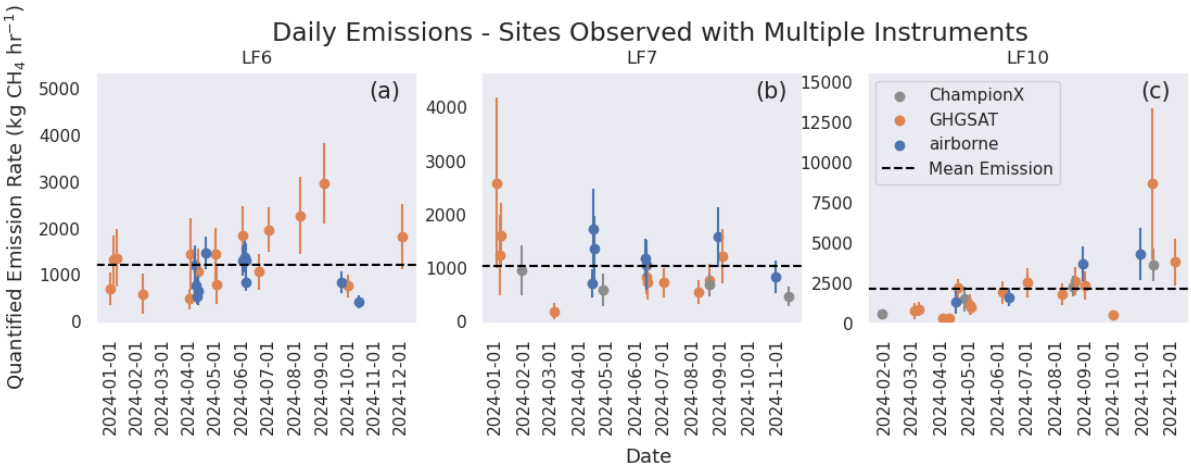

Figure S4– Daily emission estimates at California sites in 2024. Dots are colored according to instrument. (a) Emission estimates at site 6 (b) site 7 (c) site 10

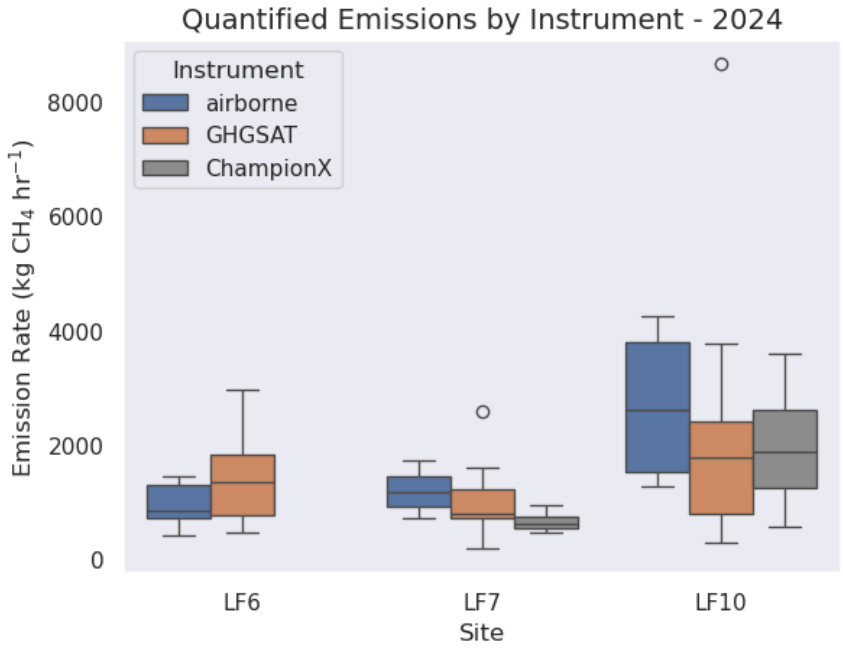

Figure S5 – Daily emission estimates at three California sites in 2024. Box plots are colored by instrument.

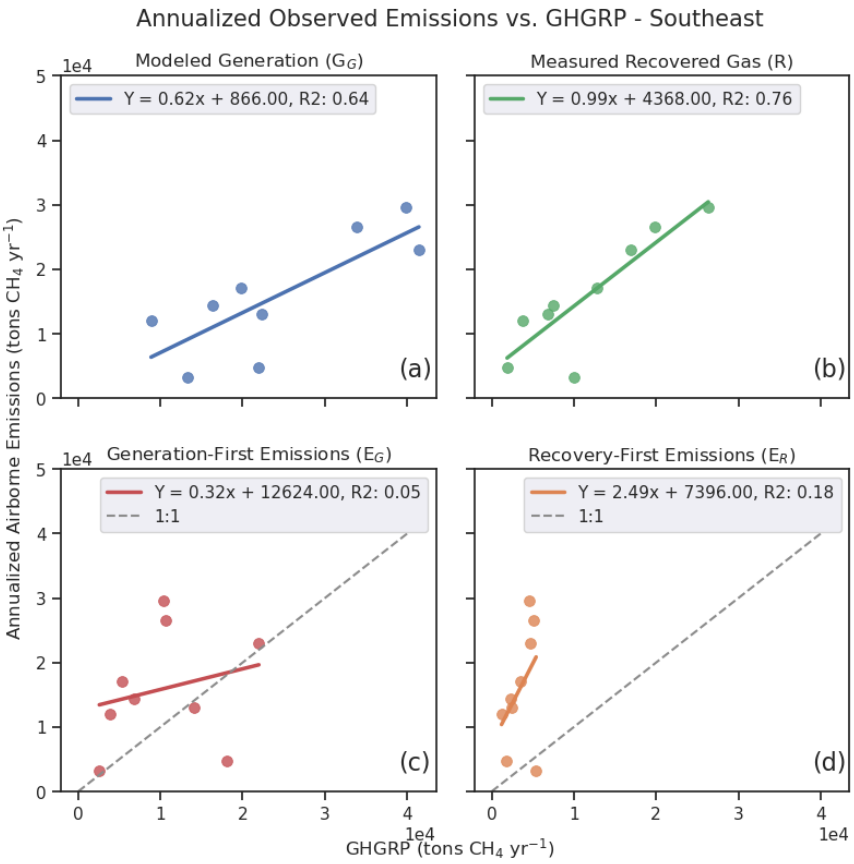

Figure S6 – Observed emissions at Southeast sites vs values reported to the GHGRP in 2022 (a) Observed annualized emissions compared to generation-first methane generation (G_G) (b) Observed annualized emissions compared to measured recovered gas (R) (c) Observed annualized emissions compared to Generation-First emissions (E_G) (d) Observed annualized emissions compared to Recovery-First emissions (E_R)

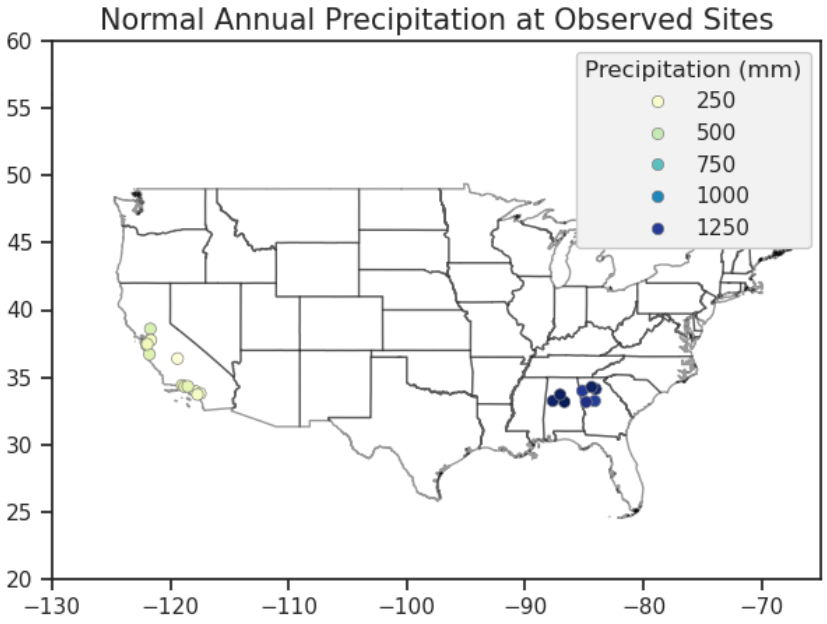

Figure S7– Annual Precipitation from NCEI 15-Year Climate Normals (2006-2020) at all airborne observed sites (NOAA NCEI, 2021)

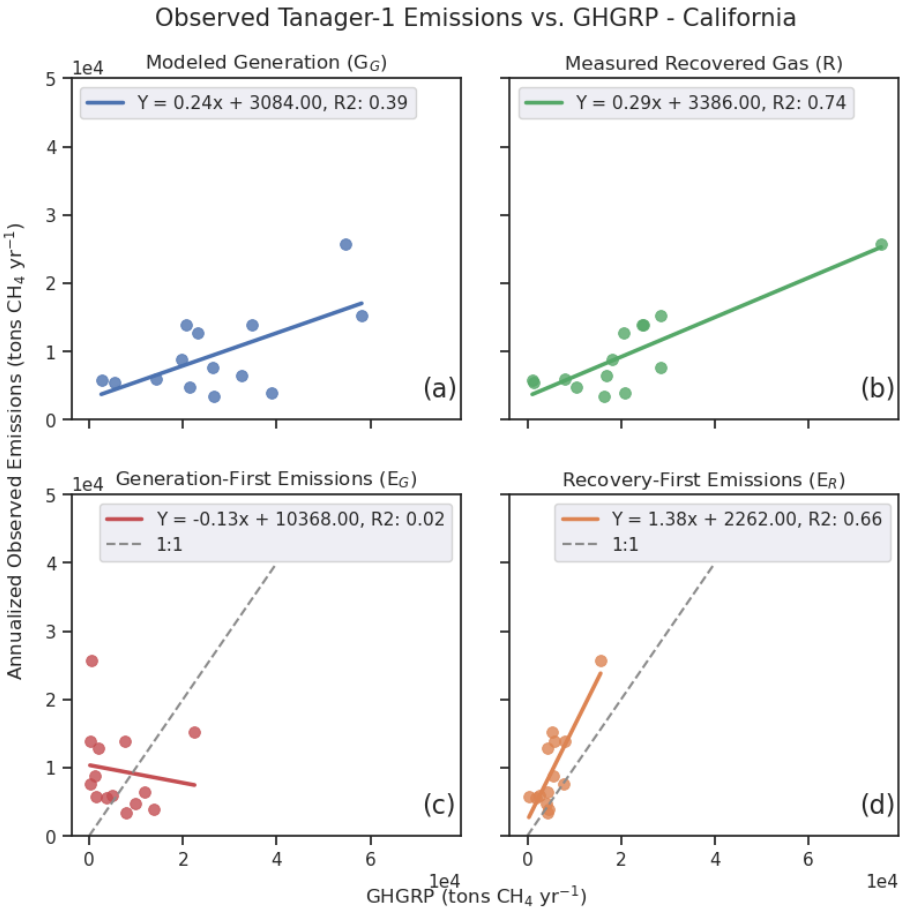

Figure S8 – Observed emissions at California sites vs values reported to the GHGRP in 2023 (a) Observed annualized emissions compared to generation-first methane generation (G_G) (b) Observed annualized emissions compared to measured recovered gas (R) (c) Observed annualized emissions compared to Generation-First emissions (E_G) (d) Observed annualized emissions compared to Recovery-First emissions (E_R)

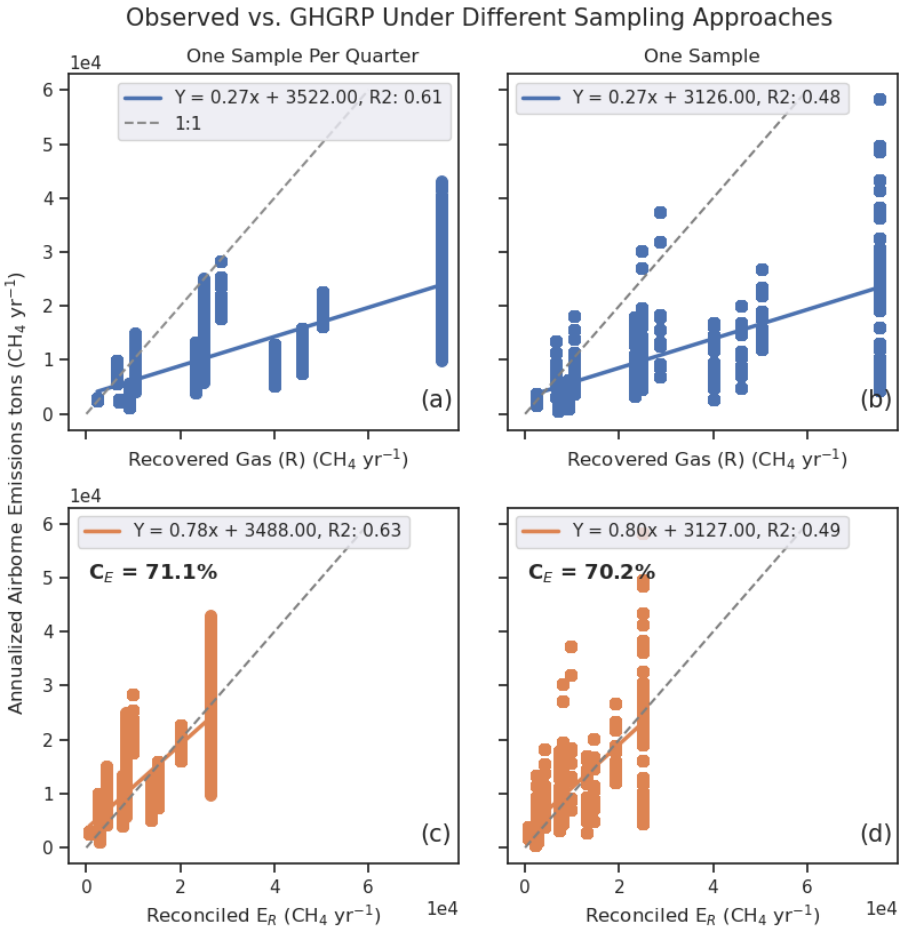

Figure S9 – (a) Annualized emissions under once per quarter sampling approach vs Recovered Gas (R) (b) Annualized emissions under single sampling approach vs Recovered Gas (R) (c) Annualized emissions under once per quarter sampling approach compared to Recovery-First emissions after applying empirical collection efficiency derived from all sampled iterations (d) Annualized emissions under single sampling approach compared to Recovery-First emissions after applying empirical collection efficiency derived from all sampled iterations

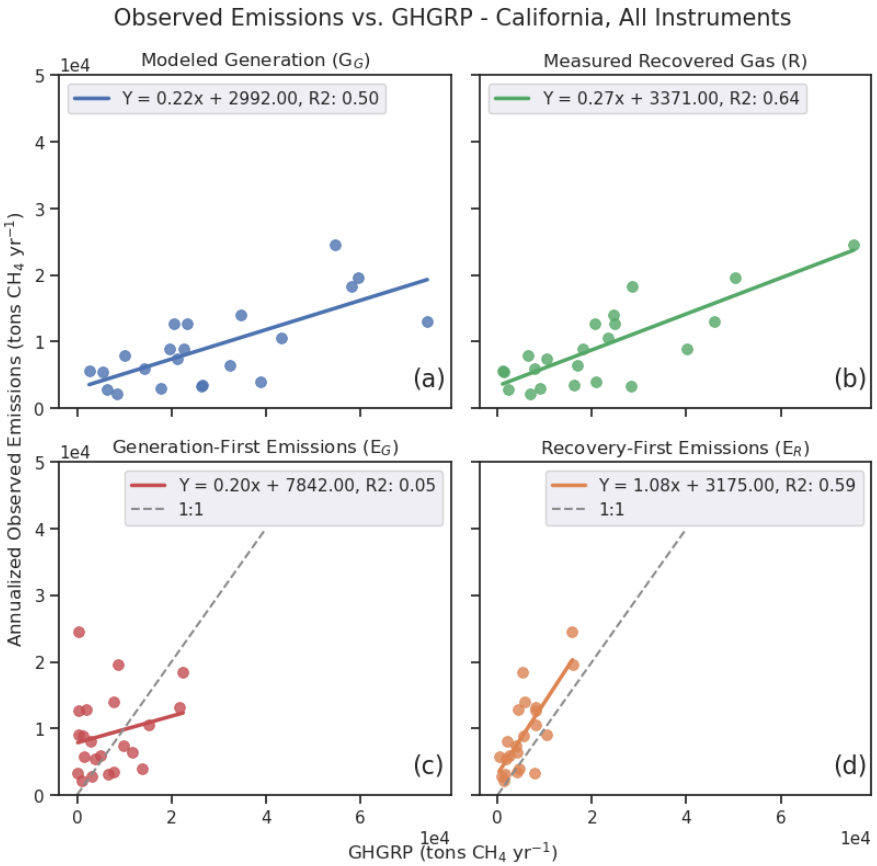

Figure S10– Observed emissions at California sites vs values reported to the GHGRP in 2023 (a) Observed annualized emissions compared to generation-first methane generation (G_G) (b) Observed annualized emissions compared to measured recovered gas (R) (c) Observed annualized emissions compared to Generation-First emissions (E_G) (d) Observed annualized emissions compared to Recovery-First emissions (E_R)

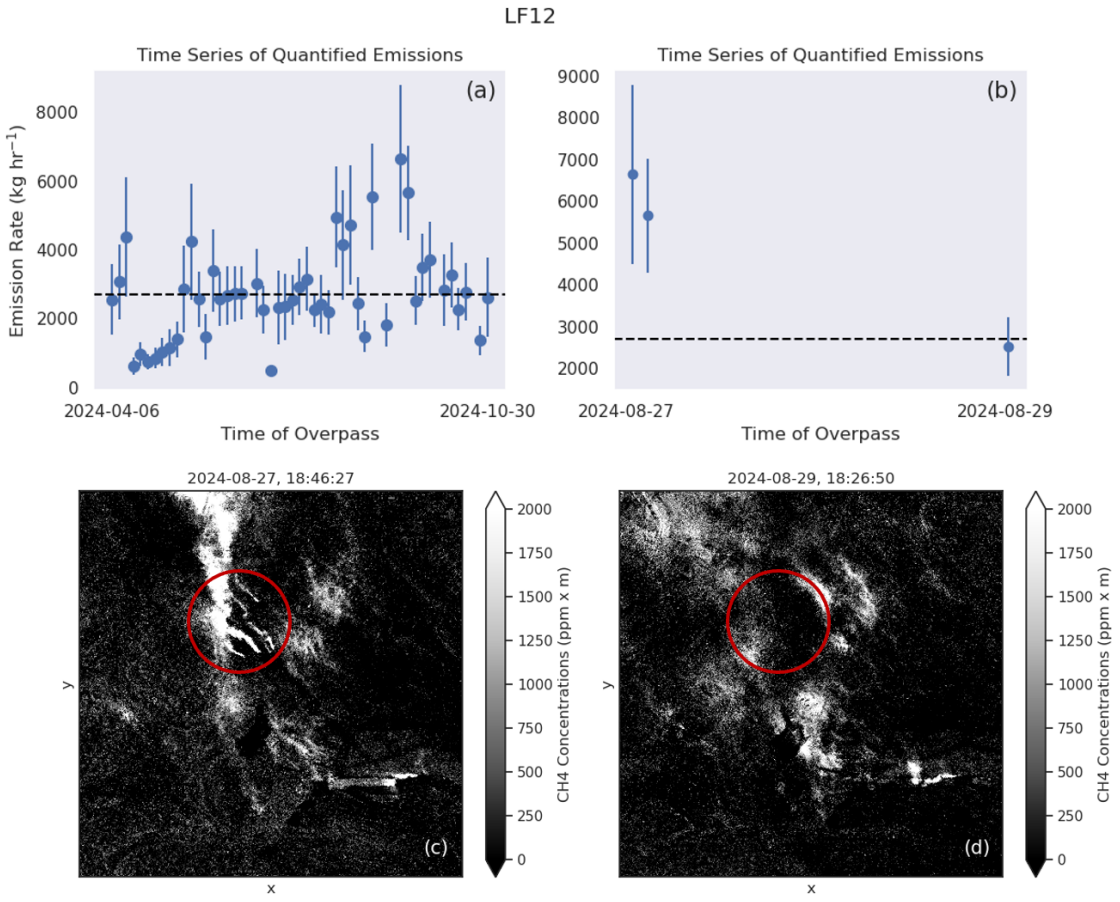

Figure S11 – (a) All quantified emission rates at LF11 (b) Quantified emission rates between August 27th and August 29th, showing high emissions on August 27th that drop significantly on August 29th (c) Methane concentration imagery taken on August 27th indicating the presence of large point sources (d) Methane concentration imagery taken on August 29th shows that sources have disappeared

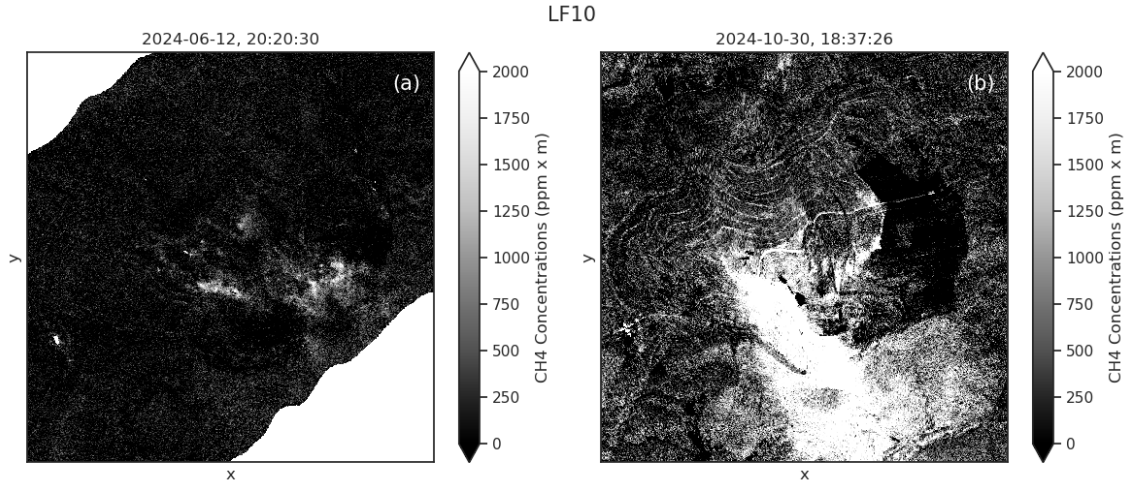

Figure S12– (a) Methane concentration imagery taken on 6/12 (b) Methane concentration imagery taken on 10/30 showing elevated concentrations